Spontaneously Formed Hydrophilic Surfaces by Segregation of Block Copolymers with Water-Soluble Blocks

Hideaki Yokoyama* and Takayuki Miyamae

Nanotechnology Research Institute, National Institute of Advanced Industrial Science and Technology, Tsukuba Central 5, 1-1-1, Higashi, Tsukuba, Ibaraki 305-8565, Japan

Seok Han and Takashi Ishizone

Department of Organic and Polymeric Materials, Graduate School of Science and Engineering, Tokyo Institute of Technology, 2-12-1, Ookayama, Meguro-ku, Tokyo 152-8552, Japan

Keiji Tanaka[†] and Atsushi Takahara[‡]

Department of Applied Chemistry and Institute for Materials Chemistry and Engineering, Kyushu University, Fukuoka 812-8581, Japan

Naoya Torikai

Neutron Science Laboratory, KEK, 1-1 Oho, Tsukuba, Ibaraki 305-0801, Japan

Received March 7, 2005; Revised Manuscript Received April 12, 2005

ABSTRACT: A block copolymer of deuterated polystyrene (dPS) and 2-[2-(2-methoxyethoxy)ethoxy]ethyl methacrylate (PME3MA) spontaneously exposes the PME3MA block, which is soluble in water, to the surface in a vacuum. dPS−PME3MA mixed with polystyrene (PS) segregates to the PS surface and changes the hydrophobic PS surface into hydrophilic surface. Neutron reflectivity, X-ray photoelectron spectroscopy, and dynamic secondary ion mass spectrometry probe the surface segregation of dPS−PME3MA to the surface of PS due to its PME3MA block. Sum-frequency generation vibrational spectroscopy detects exclusively the triethylene oxide (3EO) side chains of PME3MA regardless of a small fraction of dPS−PME3MA in the mixture, suggesting the conformation of the side chains influencing the segregation behavior. Because of the amphiphilic character of the methoxy-terminated 3EO side chains, the PME3MA block exposes the terminal methyl groups of the side chains to the surface to reduce the free energy of the system. However, such a hydrophobic methyl surface layer barely covers the EO part of the side chains; the surface quickly reconstructs and becomes hydrophilic upon contact with water. This is a technologically important demonstration of converting a hydrophobic polymer surface to a hydrophilic surface just by adding a small amount of block copolymer.

Introduction

Water-soluble polymers have been attracting considerable attention for biomedical applications. A number of outstanding articles, reviews, and books have covered the present challenges and future aspects of biomedical polymeric materials.[1] In particular, protein adsorption plays an important role in a variety of biological processes.[2] There are also many important technological applications that require controlling protein adsorption.[3] Poly(ethylene oxide) (PEO) is a typical example of the water-soluble biologically inert polymers which promote good blood compatibility by preventing the adsorption of proteins.[1,4] Poly(ethylene oxide) (PEO) is a typical example of the water-soluble biologically inert polymers which promote good blood compatibility by preventing the adsorption of proteins while it has been reported that PEO fails to show blood compatibility in vivo.[5] A variety of methods of partitioning PEO to the solid surfaces have been studied.[1,6] Attaching a water-soluble polymer to a solid surface aims to utilize the elastic repulsion of the polymer coils swollen in water and to hinder the underlaying hydrophobic surface from adhering of proteins, platelets, and cells.[7]

A layer of polymer chains attached to a solid surface is called a polymer brush, which has been studied extensively due to its unique properties.[8] Preparation of a polymer brush is categorized into three methodologies, which are physisorption, "grafting to", and "grafting from" approaches. The "grafting to" approach is typically achieved by chemically attaching a functional polymer to a solid surface. The surface must have been functionalized prior to the grafting reaction. The "grafting from" approach is more elaborate polymerization initiated from a solid surface. Those posttreatments ("grafting to" and "grafting from") may not be compatible with industrial processes, especially for applications in complex geometries. Physisorption, spontaneous adsorption of a hydrophilic polymer in water, is the simplest method among those; however, the physisorbed polymer can often be displaced from the surface. An alternative methodology of fixing a polymer onto a solid surface is either physical[9] or chemical[10] cross-linking of a polymer. A cross-linked layer of a water-soluble polymer is called a hydrogel, which is known to provide good blood compatibility. However, still good adhesion of a hydrogel to a solid surface is required.

Spontaneous segregation of a block copolymer with a hydrophobic block can produce a hydrophobic surface. A block copolymer with a hydrophobic block, typically a fluorinated block, in a mixture with a homopolymer spontaneously segregates to the surface to reduce the surface tension and forms a monolayer of the block

[†] Department of Applied Chemistry.
[‡] Institute for Materials Chemistry and Engineering.
* To whom correspondence should be addressed. E-mail: yokoyama@ni.aist.go.jp.

10.1021/ma050473w CCC: $30.25
Published on Web 05/12/2005

Scheme 1. Chemical Structure of Poly{(deuterated styrene)-*block*-2-[2-(2-methoxyethoxy]ethoxy]ethyl methacrylate} (dPS−PME3MA)[a]

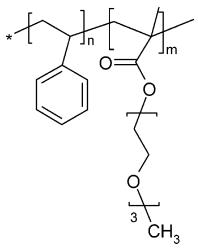

[a] Styrene block is fully deuterated (C_8D_8). The number-average molecular weights of dPS and PME3MA are 10 500 and 7200, respectively. The polydispersity index M_w/M_n is 1.06.

copolymer at the surface.[11] The surface compositions and properties are entirely altered by adding a tiny amount of such a block copolymer. This methodology does not work in general for a hydrophilic block copolymer due to the relatively high surface energy of the hydrophilic (or more specifically water-soluble) block which tends to be repelled from the surface and embedded into the bulk. Even if being placed on a hydrophobic polymer surface, a water-soluble block can bury itself under the surface in order to reduce the free energy of the system.[12] If this surface is placed into water, fouling may occur before the surface is able to reorganize and partition the water-soluble block back into water. However, a few exceptions have been reported. Kajiyama et al. revealed that the polymethacrylate with the side chains of methoxy-terminated oligo ethylene oxide (EO) enriched the concentration of EO at the surface and reduced the contact angles of water.[13] Walton et al. observed the similar surface segregation of random copolymers of methyl methacrylate and the methacrylate with methoxy-terminated oligo EO side chains.[14] The methyl terminations of EO side chains are apparently important for the spontaneous surface enrichment of the hydrophilic part of the polymers. The methacrylates with EO side chains without methyl termination such as poly(2-hydroxyethyl methacrylate), poly[(diethylene oxide) methacrylate], and poly[(triethylene oxide) methacrylate] are known to stay away from the surfaces.[14,15]

Using the method reported previously,[16] we synthesize poly{(deuterated styrene)-*block*-2-[2-(2-methoxyethoxy)ethoxy]ethyl methacrylate} (dPS−PME3MA) (Scheme 1). Deuterated styrene allows us to use nuclei-sensitive techniques to trace the distribution of dPS. The methacrylate with three units of EO (3EO) with a methyl terminus, ME3MA, is chosen for this study since PME3MA is the water-soluble polymethacrylate constituted with the least number of EO units with a methyl terminus. The polymethacrylate with two units of EO and a methyl terminus is not soluble in water at 26 °C or above and therefore is not suitable for biomedical applications. The surfaces of the neat dPS−PME3MA and the mixtures of dPS−PME3MA and polystyrene (PS) are characterized by X-ray photoelectron spectroscopy (XPS), dynamic secondary ion mass spectrometry (DSIMS), neutron reflectivity (NR), contact angle (CA), and sum-frequency generation vibrational spectroscopy (SFG). The spontaneous segregation of the dPS−PME3MA copolymer in the dPS−PME3MA/PS mixtures is quantitatively evaluated. SFG reveals that the methyl termini of the 3EO side chains exclusively cover the surface to be pseudo-hydrophobic and hence drive the segregation of the dPS−PME3MA copolymer to the surface of the mixture. The contact angle of water on the dPS−PME3MA/PS mixtures significantly decreases immediately after contact, which is the evidence of surface reconstruction and formation of a hydrophilic surface. Consequently, the segregation of dPS−PME3MA to the surface spontaneously convert hydrophobic PS surfaces to practically hydrophilic surfaces.

Experimental Section

Materials. The block copolymer used in this study was synthesized using anionic polymerization described previously.[15,16] ME3MA monomer was synthesized by a reaction of methacryloyl chloride with 3EO monomethyl ether in the presence of triethylamine in diethyl ether. The anionic polymerization of deuterated styrene (Cambridge Isotope Laboratories, Inc.) was initiated by *sec*-buthyllithium at −78 °C in tetrahydrofuran for 10 min. Subsequently, 1,1-diphenylethylene (DPE) and Et_2Zn were added to the living polystyrene to decrease the nucleophilicity of the anion and to avoid a side reaction with methacrylates. The DPE-capped living polystyrene initiated ME3MA monomer in the presence of Et_2Zn. The number-averaged molecular weights (M_n) of dPS and PME3MA were 10 500 and 7200, respectively. The polydispersity index (PDI) was 1.06 for dPS−PME3MA. A polystyrene (M_n = 99 100 and PDI = 1.08) was purchased from Polymer Source Inc. The volume fraction of PME3MA is calculated to be 0.41 provided that the densities of PS and PME3MA are both 1.06.

The films for NR, XPS, and DSIMS were prepared by spin-casting of toluene solutions of dPS−PME3MA or dPS−PME3MA/PS mixtures on silicon wafers. The silicon wafers were rinsed with toluene before use. The thickness of the dPS−PME3MA film for NR was 80 nm whereas the films for XPS, DSIMS, and CA were set to ≈300 nm. The films were annealed at 140 °C in a vacuum for 12 h unless otherwise stated.

X-ray Photoelectron Spectroscopy. XPS spectra were acquired on a PHI Quantum 2000 spectrometer equipped with a hemispherical capacitor analyzer using a monochromated X-ray from Al Kα. A binding energy scale of the instrument was calibrated by setting Au $4f_{7/2}$ to 84.0 eV, Cu $2p_{3/2}$ to 932.6 eV, and Ag $3d_{5/2}$ to 368.3 eV. A chamber pressure during the measurements was maintained at ca. 1×10^{-7} Pa. An X-ray beam operated at 20 W and focused onto ca. 100 μm in diameter rastered over a 500 μm by 500 μm square area. We obtained sharp C 1s and O 1s peaks without neutralization: a small shift in bonding energy was rescaled using the C 1s peak as a standard to 284.8 eV. High-resolution scans of C 1s and O 1s regions were acquired with a pass energy of 35.8 eV at θ, which is defined as the angle between the surface plane and the direction toward the analyzer. θ of 10, 15, 20, 25, 30, 35, 40, 45, 55, 65, and 85° were chosen for the angular dependence measurements. An analyzer aperture was introduced to limit a range of takeoff angles to ±4°. An XPS intensity from the depth, z, decays exponentially due to an inelastic scattering process with an electron escape depth, λ_i; therefore, the XPS intensities are given by the Laplace transform of the atomic fraction, $\Phi_i(z)$, of element i. By taking the intensity ratio of O 1s and C 1s simultaneously measured at the same angle, the intensity ratio can simply be written by

$$\frac{I_{O\,1s}}{I_{C\,1s}} = \frac{I^{\circ}_{O\,1s}}{I^{\circ}_{C\,1s}} \frac{\lambda_{O\,1s}}{\lambda_{C\,1s}} \frac{\int_0^{\infty} \Phi_{O\,1s}(z) \exp\left(-\frac{z}{\lambda_{O\,1s}}\right) dz}{\int_0^{\infty} \Phi_{C\,1s}(z) \exp\left(-\frac{z}{\lambda_{C\,1s}}\right) dz} \quad (1)$$

The electron escape depth, λ_i, of an element, i, is given by

$$\lambda_i = \lambda^{\circ}_i \sin\theta \quad (2)$$

where λ°_i is an inelastic mean free path (IMFP) of element i. On the basis of the kinetic energy dependence of IMFP proposed by Ashley,[17] $\lambda^{\circ}_{C\,1s}$ and $\lambda^{\circ}_{O\,1s}$ were computed to be 3.5

and 2.9 nm, respectively, for the incident X-ray Al Kα with a kinetic energy of 1486.6 eV. The atomic sensitivity factors for C 1s, $I^{\circ}_{C\,1s}$, and for O 1s, $I^{\circ}_{O\,1s}$, were 0.314 and 0.733, respectively, given by the manufacturer. Equations 1 and 2 were used to fit the data to extract the depth profiles by the scheme described previously.[18] The depth profiles were integrated to obtain the surface excesses of dPS−PME3MA.

Dynamic Secondary Ion Mass Spectrometry. Dynamic SIMS measurements were performed with an Atomica SIMS 4000 using a 4 keV, ca. 30 nA beam of O_2^+ ions at 45° off normal incidence, which was rastered over a 0.09 mm^2 region. The surface of each specimen was covered with a sacrificial layer of deuterated polystyrene (dPS) followed by sputter coating of gold with a thickness of ca.∼20 nm to reduce electric charge-up during the SIMS measurement. Charge neutralization using electron flood gun was not employed. Negative ions of H, ^{2}H (D), C, and Si were monitored as a function of time from an electrically gated area which is less than 25% of the rastered area. By measuring the thickness of the polymer film using an ellipsometer and assuming a steady rate of sputtering, sputtering time was converted into depth. We converted the intensities of the negative ions of D into the volume fraction of the copolymer as a function of depth. The depth profiles are integrated to obtain the surface excesses of dPS−PME3MA.

Contact Angle Measurements. Contact angles of water were measured using a contact angle meter CA-V (Kyowa Interface Science Co., Ltd.). A water droplet of 5 μL was placed on the specimens, and another 5 μL was added to measure advancing angles. Receding angles were measured by extracting the water from the needle. A charge coupled device camera was used to capture the images of advancing and receding water droplets for the determination of the contact angles.

Small-Angle X-ray Scattering (SAXS). SAXS profiles were obtained using an X-ray diffractometer (Rigaku Ultrax 4153A 172B). A Cu Kα radiation (λ = 1.54 Å) was utilized for an incident X-ray beam. A scattered X-ray was detected with an imaging plate placed approximately 600 mm behind the specimen. The two-dimensional images were azimuthally averaged to obtain the plots of the intensity vs the scattering angle, 2θ. All the measurements were performed at room temperature.

Neutron Reflectivity. Neutron reflectivity (NR) measurements were carried out using an advanced reflectometer for interface and surface analysis (ARISA) on H5 beamline of Neutron Science Laboratory, High Energy Accelerator Research Organization. A neutron beam with a range of wavelengths from 0.12 to 0.4 nm was used. The corresponding q (= $(4\pi/\lambda)\sin\theta$) range is $0.08 < q < 1$ nm^{-1}, where λ is a wavelength and θ is an angle of incident and reflected neutron beams respective to the surface plane with an angular resolution $\Delta\theta/\theta < 7.5\%$. The detail of ARISA is found elsewhere.[19] The scattering length density along the depth direction was computed from the reflectivity using the Spreadsheet Environmental Reflectivity Fitting software.[20]

IR−Visible SFG Spectroscopy. In IR−visible SFG experiments, a mode-locked Nd:YAG laser (PL2143D, EKSPLA) at 1064 nm with 25 ps pulse width and 10 Hz repetition rate was employed for a master light source. A tunable IR beam in the range of 1200−4300 cm^{-1} was generated by a $AgGaS_2$ crystal by different frequency mixing of the fundamental of the Nd:YAG laser with the output of an optical parametric oscillator/amplifier (OPO/OPA) system, which was composed of a LiB_3O_5 crystal, pumped by the third harmonics of the laser. The visible and IR beams were overlapped at a sample surface with the incident angles of 70 and 50°, respectively. The pulse energy and spot size of the tunable IR were 0.2−0.3 mJ and 0.2−0.3 mm in diameter, respectively. The spectral resolution was 6 cm^{-1}. SFG spectra were recorded with various polarization combinations of the SFG, visible, and IR pulses with respect to the plane of incidence. The polarization combination is abbreviated in the order such as ssp for s-polarized SFG, s-polarized visible, and p-polarized IR pulses. The details of the experimental setup have been described elsewhere.[21]

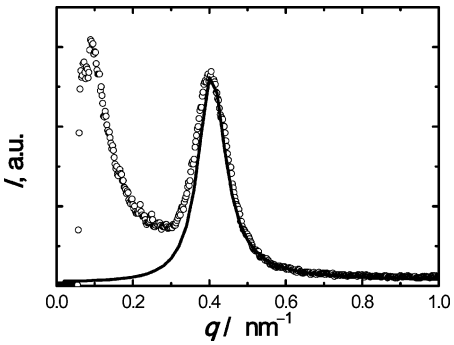

Figure 1. Small-angle X-ray scattering profile of dPS−PME3MA block copolymer. Intensity I is plotted in an arbitrary unit against q defined by $q = (4\pi/\lambda)\sin\theta$. The circles are representing data points, and the line is the fit by random phase approximation described in the text.

Films of ca. 300 nm for the SFG experiments were prepared by spin-casting of a toluene solution of the polymer mixture on a glass plate. To confirm that the SFG spectra did not originate from the polymer/glass interface but from the polymer surface, the spectra from the polymer films of a few different thicknesses were acquired. They were identical within an experimental error (not shown here); we, therefore, measured SFG spectra of polymer surfaces.

Results and Discussion

Bulk and Surface Structures of Neat dPS−PME3MA. It has been revealed that PME3MA is a water-soluble polymer having the lower critical solution temperature (LCST) of 52 °C.[16] The block copolymer of dPS and PME3MA may cause microphase separation due to the difference in solubilities. Our previous study[15] showed, however, that the methyl termini of EO side chains significantly reduced the interaction with PS and hence altered the phase behavior. Shown in Figure 1 is the small-angle scattering profile of dPS−PME3MA annealed at 140 °C for 10 h and quenched to room temperature. q is defined as $q = (4\pi/\lambda)\sin\theta$, where the angle between the incident and scattered X-rays is 2θ. A broad single peak in the profile clearly indicates that dPS−PME3MA is in a disorder phase, and the q at the peak top, q_{max}, is inversely proportional to the wavelength of the fluctuation. We attempt to extract the Flory χ parameter from the fluctuation peak using a random phase approximation (RPA) introduced by Leibler.[22] A structure factor, $S(q)$, is calculated by

$$S(q) = N/[F(x) - 2\chi N] \tag{3}$$

where $F(x)$, the Debye function $g_1(f,x)$, and x are defined as

$$F(x) = g_1(1,x)/\{g_1(f,x)\,g_1(1-f,x) - {}^1/_4[g_1(1,x) - g_1(f,x) - g_1(1-f,x)]^2\} \tag{4}$$

$$g_1(f,x) = 2[fx + \exp(-fx) - 1]/x^2 \tag{5}$$

and

$$x = q^2 R_g^{\,2} \tag{6}$$

respectively, with a radius of gyration, R_g, of a block copolymer with N monomers and volume fraction f. Since the segmental length of PME3MA is not available, we used R_g as an independent fitting parameter in addition to χ. The scattered intensity is given by $I(q) = CS(q)$, where the proportional constant C is also used

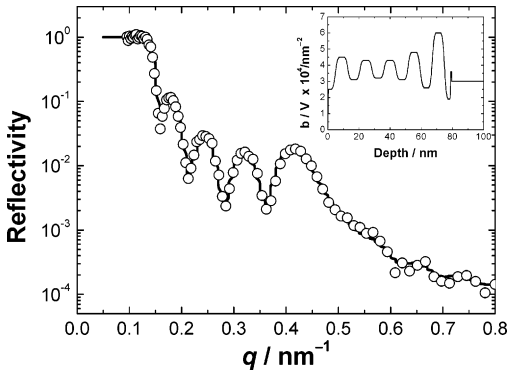

Figure 2. Neutron reflectivity of the neat dPS−PME3MA block copolymer on a silicon substrate. The reflectivity is plotted against q defined by $q = (4\pi/\lambda) \sin \theta$. The solid line is a fit using a model depth profile of neutron scattering length density b/V shown in the inset.

as a fitting parameter. A fit of the RPA is shown as a solid line in Figure 1, in which only the higher q side of the peak is used for the fit to avoid the influence of the tail of direct beam. For the total number of segments $N = 131$ and volume fraction $f = 0.41$, χ is estimated to be 0.079 at 140 °C.[23] It should be noted that the χ parameter is a rough estimate and rather gives the upper limit of the possible χ range since the fluctuation may have grown slightly during the temperature quench. R_g was fitted to 4.8 nm, which is reasonably close to an estimated R_g of 4.5 nm by assuming R_g/(molecular weight)$^{1/2}$ of PME3MA is equal to that of PS.[24] The estimated χ will be used to discuss the critical micelle concentration of dPS−PME3MA in the PS matrix in the section below. The χ is surprisingly small despite the difference of the solubilities of PME3MA and PS in water. It seems that the interaction of PME3MA with PS is screened by the presence of the methyl termini: PS may not have a direct contact with the EO in the interior of the side chains while a small molecule like water can easily penetrate into the interior of the side chains and interact with the EO.

It is known that a block copolymer even in a disorder phase forms a layered structure induced by the difference in the surface energies of the blocks.[25] Therefore, dPS−PME3MA in a disorder phase may not have a homogeneous composition at the surface. We measured a depth profile of a dPS−PME3MA thin film using neutron reflectivity (NR) to reveal a surface induced structure. The reflectivity of the film and its model depth profile which fits the reflectivity data are shown in Figure 2 and its inset. The periodic, named as the Kiessig, fringes represent the total thickness of the film while the broad peak appearing around q of 0.43 nm^{-1} corresponds to the periodic structure of dPS−PME3MA perpendicular to the surface. Since the q_{max} of the SAXS profile in Figure 1 agrees reasonably well with the q_{max} in the reflectivity, the layered structure induced by the surface and interface has the same length scale as the fluctuation. The profile of a scattering length density, b/V, in which dPS has a higher value of b/V, clearly shows decaying oscillation from the surface and the silicon substrate. The depletion layer of b/V at the surface clearly indicates that the PME3MA block preferentially covers the surface. Despite the dPS−PME3MA block copolymer in a disorder phase due to the fairly small χ and low molecular weight, the surface is sufficiently covered by the water-soluble PME3MA blocks. This effect can be easily enhanced by increasing

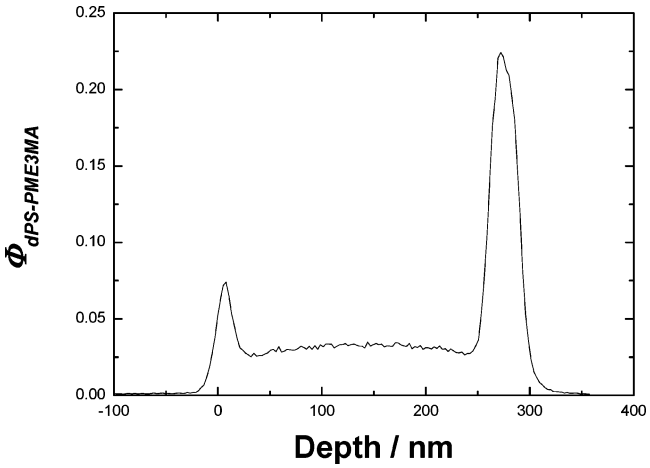

Figure 3. DSIMS depth profile of the dPS−PME3MA block copolymer in the PS homopolymer after annealing at 140 °C for 12 h. $\Phi_{dPS-PME3MA}$, the concentration of dPS−PME3MA in PS, was estimated from D^- intensity. The peaks at the depths of 0 and 280 correspond to the surface segregation and interfacial segregation to native oxide of silicon, respectively.

the molecular weight of the dPS−PME3MA block copolymer.

The spontaneous enrichment of PME3MA at the surface is very important for controlling hydrophilicity of a surface, especially for biotechnological applications. The surface PME3MA layer is expected to be highly swollen immediately after contact with water due to the solubility of the PME3MA block in water as shown later in this paper, and the biocompatibility will be reported in a separate paper.

Segregation of dPS−PME3MA in Mixtures with PS. As a more severe test of the spontaneous formation of hydrophilic surfaces using dPS−PME3MA, we blend a small amount of dPS−PME3MA into a homo-PS to alter the surface properties of PS. It is technologically important that adding a small amount of a copolymer can modify the surface hydrophilicity. A surface segregation isotherm of a block copolymer in a homopolymer matrix has been studied experimentally[11] and theoretically[26] while those studies are intended for a segregation of the hydrophobic part of the copolymer to the surface. We evaluate quantitatively the segregation behavior of dPS−PME3MA, providing a hydrophilic surface instead of a hydrophobic surface using the theories of segregation to extract the thermodynamic parameters. A series of mixtures of PS and dPS−PME3MA were spun-coat onto silicon wafers. The specimens were annealed at 140 °C for 12 h. Selected specimens were annealed for 24 h to check whether the surface had reached equilibrium, but no significant difference between 12 and 24 h was found (not shown here) and hence the surface had been equilibrated in 12 h. The surfaces of the specimens were characterized using XPS and DSIMS. The surface excess, z^*, which is the integrated thickness of a block copolymer layer, was obtained from the angular dependent XPS intensities by the method described in the Experimental Section. Another set of z^* was obtained from the depth profiles of dPS using DSIMS. An example of the depth profiles obtained using DSIMS is shown in Figure 3. The peaks at depth of 0 and 280 nm clearly indicate the excesses of dPS−PME3MA at the surface and interface with the silicon wafer, respectively. By integrating the corresponding surface segregation peak, the surface excess can be calculated. The surface excesses obtained by two independent methods

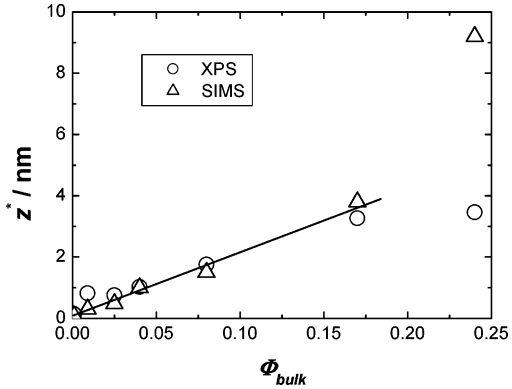

Figure 4. Segregation isotherm of the dPS−PME3MA block copolymer in the PS homopolymer. The surface excess, z^*, was estimated both from XPS and DSIMS measurements and plotted against the volume fraction of dPS−PME3MA in bulk, Φ_{bulk}.

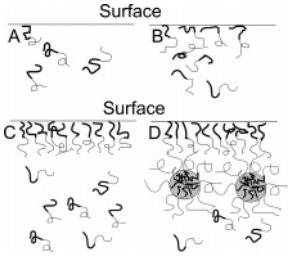

Figure 5. Schematic illustrations of segregation mechanism. For simplicity, homopolymers are not drawn. The thicker curves represent PME3MA blocks. At low concentrations in panels A and B, the segregation isotherm linearly depends on the concentration in bulk. Further segregation is prevented by the brush layer at the surface as shown in panel C, and the segregation isotherm becomes nonlinear. Micelles start to form in bulk and stick to the brush layer: the concentration of free block copolymer chains and hence the chemical potential driving the segregation barely depend on the amount of the block copolymer added to the system.

are plotted in Figure 4 as a function of the volume fraction of dPS−PME3MA block copolymer in bulk, Φ_{bulk}. Φ_{bulk} is slightly less than the average volume fraction in the mixture due to the segregation to the surface and interface in the films of finite thickness. Therefore, we estimated the values of Φ_{bulk} from the volume fractions in the middle of the films using the DSIMS depth profiles after the segregation completed. The XPS and DSIMS measurements provide the same z^* within an experimental error, except for the data at the highest Φ_{bulk}. The dependence of z^* on Φ_{bulk} is well approximated by a linear dependence in the concentration range of $\Phi_{bulk} < 0.2$. This linear dependence is clear evidence of the dPS−PME3MA block copolymer forming neither micelles nor dense surface brushes. This situation is schematically drown in Figure 5A,B. In the absence of micelles the reference state of the chemical potential for the segregation to the surface is well approximated by the mean field theory, in which the PME3MA block is assumed to be in full contact with PS. Moreover, the linear dependence of z^* on Φ_{bulk} indicates that the segregated dPS−PME3MA chains on the surface do not strongly interact; the segregated dPS−PME3MA chains do not form a highly extended brush excluding the approaching block copolymer chains from the surface, which is schematically shown in Figure 5C. One can derive a linear relation of z^* and Φ_{bulk} with the effective χ parameter, χ_{eff}, for the surface segregation by considering only the loss of entropy by partitioning the block copolymer chains to the surface.[26] For a small Φ_{bulk}, the segregation isotherm can be approximated by a linear relationship as in eq 7 and agrees well with the experimentally observed isotherm in Figure 4.

$$z^* = (\pi/2)R_g(\chi_{eff}N_{PME3MA})^{-1/2}\exp(\chi_{eff}N_{PME3MA})\Phi_{bulk} \quad (7)$$

$$\chi_{eff} = \chi_{PME3MA-PS} - \chi_{PME3MA-surface} \quad (8)$$

Even with the small $\chi_{PME3MA-PS}$ that makes the dPS−PME3MA block copolymer miscible in PS matrix, the favorable surface interaction of PME3MA, χ_{eff} (χ_{eff} = 0.022), drives dPS−PFME3MA to segregate to the surface. It should be noted that χ_{eff} of 0.022 is not a large number; the driving force for the segregation per segment is not very strong. The segregation is enhanced by increasing the molecular weight for practical applications being controlled by $\chi_{eff}N_{PME3MA}$, as in eq 7.

What is the discrepancy of the surface excesses obtained by XPS and DSIMS at the highest concentration? The surface sensitivities of DSIMS and XPS are different: while XPS picks up information of less than 10 nm from the surface and less sensitive with increasing depth, DSIMS integrates over with its limited resolution (ca. 10 nm). If a subsurface structure is present underneath the surface segregation layer with a separation less than 10 nm, SIMS cannot distinguish those layers. At Φ_{bulk} of 0.2 or higher, dPS−PME3MA may exceed its critical micelle concentration (cmc), Φ_{cmc}, form micelles in the PS matrix and stick to the surface brush layer as schematically shown in Figure 5D. The reason for this speculation is the following. A simple estimation of Φ_{cmc} using Leibler's theory[27] is shown in eqs 9 and 10.

$$\mu_{cmc} = (3/2)^{4/3}f^{4/9}(1.74f^{-1/3} - 1)^{1/3}(\chi N)^{1/3} \quad (9)$$

$$\Phi_{cmc} = \exp(\mu_{cmc} - f\chi N) \quad (10)$$

The block fraction and the chemical potential for critical micelle formation are denoted as f and μ_{cmc}, respectively. For the set of parameters, $N = 131$, $\chi = 0.079$, and $f = 0.41$, we obtain $\Phi_{cmc} = 0.23$. The theory predicts that dPS−PME3MA does not form micelles in the concentration range of $0 < \Phi_{bulk} < 0.23$. This theoretical prediction is in good agreement with the linear dependence of z^* on Φ_{bulk}, which indicates that neither micelles are formed nor the surface are fully occupied by the stretched block copolymer, in the isotherm of Figure 4. When Φ_{bulk} approaches 0.23, z^* estimated by XPS, which is likely to be the true z^*, shows a sign of saturation. Once micelles are formed in the blend, the micelles have a tendency to stick to the surface and interface to reduce the interfacial tension between the corona of the micelles and the surrounding homopolymer with the molecular weight higher than that of the block copolymer.[28] Therefore, DSIMS fails to evaluate z^* accurately at the Φ_{bulk} higher than Φ_{cmc}. The discrepancy between two experimental methods rather clearly indicates Φ_{cmc} of the dPS−PME3MA in PS matrix. This cmc estimated from this discrepancy reasonably agrees with the theoretical prediction using the interaction parameter estimated from the fluctuation peak of SAXS profile.

Our strategy of using spontaneous segregation of block copolymers to the surface has some distinct

advantage over traditional surface modifications. Since this segregation process is thermodynamic process toward equilibrium, the surface structure will not reconstruct over time. The trend is the same or even enhanced when the environment becomes hydrophilic. A similar approach using a blend of linear polymer and a random graft copolymer with oligo EO side chains has been investigated.[4] However, such graft copolymers with oligo EO side chains become water-soluble if too many or too long EO chains are introduced, while the blood compatibility requires large number of EO chains and/or long EO side chains. The number and the length of EO must be chosen in such a way that the graft copolymer is insoluble in water but still shows a blood compatibility. In our methodology, water-soluble PME3MA blocks are anchored with the dPS blocks to the surface of homo PS. Therefore, when the mixture is dipped into water, PME3MA block forms a brush extended into water and bonded to hydrophobic PS. Wetting properties of water on the surface of the mixture will be discussed later in this report.

Conformation of the Side Chains at the Air Surface: Vibrational Sum-Frequency Generation Spectroscopy. While enthalpy is, in general, the main contribution to the surface free energy, conformational entropy of a polymer near the surface is not negligible. Especially the entropy effect is significant for graft copolymers as suggested in the literature.[14] Even polystyrene can be considered as a graft copolymer with phenyl side group as revealed by SFG spectroscopy that the surface of PS is covered with phenyl groups standing perpendicular to the surface or with slight tilt.[29] The backbones of polymers are rarely seen by surface-sensitive SFG spectroscopy. The local conformation of side chains at the surface is extremely important to understand the surface properties of polymers. A methyl terminus of oligo EO plays an important role for the observed lower surface energies of oligo EO than those of PEO.[27−30] This terminus effect is enhanced when the molecular weight of EO is low; therefore, when a short EO is attached to a polymer backbone, the terminal methyl group may alter the interaction and surface properties significantly. We discuss the conformation of the 3EO side chains with methyl termini of PME3MA to understand the origin of the unique surface segregation behavior using surface-sensitive vibrational sum-frequency generation spectroscopy (SFG), which has emerged as a powerful tool for the study of the molecular structure of interfaces.[31] Recently, SFG has been applied to the studies of free surfaces of polymer substrates, alignment of surface chains,[32] chemical composition of the surface,[33] and processing induced molecular changes in the surface.[34] SFG can probe the molecular orientation at the surfaces which other surface-sensitive techniques cannot detect.

Figure 6 shows SFG spectra in 2700−3100 nm^{-1} wavenumber region with an SSP polarization combination of homo PS and the mixtures with dPS−PME3MA of 2% and 10%. P and S denote the polarized lights perpendicular and parallel to the surface, respectively. The first S, second S, and last P denote the polarizations of SFG, visible, and infrared light, respectively. From homo PS, we detected the vibrations of only phenyl ring of PS (3060−3070 nm^{-1}): no obvious vibrations of backbones of PS are found as already reported.[29] The phenyl side groups of PS exhibit five vibrational modes of C−H aromatic stretches, which are both Raman- and infrared-active. These five modes are believed to have the resonance frequencies at 3024, 3035, 3055, 3067, and 3078 cm^{-1} corresponding to ν_{20a}, ν_{7b}, ν_{7a}, ν_2, and ν_{20b} vibrational modes, respectively.[29] With the SSP polarization combination, the dominant ν_2 peak at 3067 cm^{-1} qualitatively indicates phenyl rings standing nearly perpendicular to the surface. With increasing Φ_{bulk} in the mixtures, the peak intensity of ν_2 decreases and becomes almost invisible at 10%. In addition, ν_{20a} at 3024 cm^{-1} appears at Φ_{bulk} of 2% while being negligibly small at 0 and 10%. Since ν_{20a} in SSP appears only when the phenyl groups significantly tilt from the surface normal, it can be concluded that PME3MA segregates to the surface and disturbs the alignment of phenyl groups of PS at Φ_{bulk} of 2%. However, the phenyl groups may be excluded from the surface at Φ_{bulk} of 10%. At 10% of dPS−PME3MA, the segregated PME3MA blocks dominate the spectra with no sign of phenyl groups. This disappearing of the PS signals at 10% is slightly earlier than that in the XPS and DSIMS results, in which z^* saturates at 20%. Since SFG intensities depend not only on composition but also on orientation, this discrepancy may be suggestive of the loss of orientation of a small amount of phenyl groups of PS in a majority of PME3MA at 10%. Nevertheless, the physical picture of the segregation is essentially unchanged. Using SFG, we observe systematically that the orientation of phenyl groups of PS at the surface are disturbed by the segregated PME3MA blocks and then excluded from the surface with increasing Φ_{bulk}.

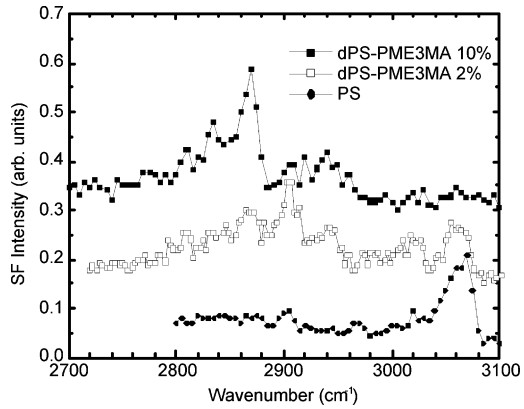

Figure 6. SFG spectra in C−H stretching vibration region with an SSP polarization combination of the PS homopolymer and the mixtures of PS and dPS−PME3MA (2%) and (10%). The sum frequency (SF) intensities are shifted vertically for clarity.

PME3MA exhibits five vibrational modes composed of the C−H stretches that are both Raman- and infrared-active. These five modes are assigned to the resonance frequencies at 2835, 2873, 2910, 2940, and 2965 cm^{-1}, corresponding to the s-OCH_3, s-OCH_2, as-CH_2, as-OCH_2, and as-OCH_3 vibrational modes, respectively.[35] The characters s and as denote symmetric and asymmetric vibrational modes, respectively. It is clearly observed that PME3MA peaks dominate the spectra with decreasing intensity of the vibrational modes of phenyl rings. Comparing the spectra at 2% and 10%, we clearly find that the dominant peak changes from 2910 to 2873 cm^{-1}. While the assignment of the peak at 2910 cm^{-1} is not well established, this peak can be as-CH_2 of the backbone. In the SFG studies of PEO and poly(2-methoxyethyl acrylate)[35] and in the spectrum at 10% of dPS−PME3MA, the peak at 2910 cm^{-1} were not clearly detected. Considering that PS and PME3MA are mixed

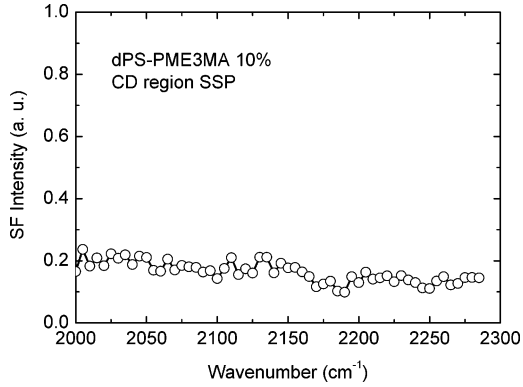

Figure 7. SFG spectrum in C−D stretching vibration region with an SSP polarization combination of the mixture of PS and dPS−PME3MA (10%). No significant peaks of C−D stretching are observed.

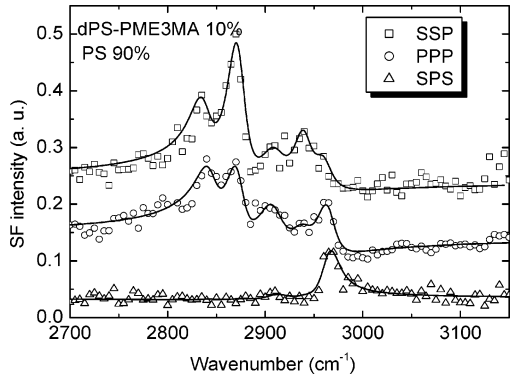

Figure 8. SFG spectra in a C−H stretching vibration region with SSP, PPP, and SPS polarization combinations of the mixture of PS + dPS−PME3MA (10%). The curves are the fits of eq A2 in the Appendix to the data. The details of the fitting procedure is described in the Appendix and Supporting Information.

at the surface of the 2% mixture, the backbones of PS and/or PME3MA may be exposed to the surface to be detected by SFG. In the 10% mixture, the peaks at 2837 cm^{-1} of s-OCH_2 and at 2835 cm^{-1} of s-OCH_3 dominate the spectra, which clearly illuminate the surface of the mixture dominated by the side chains of PME3MA similar to the surfaces of the polyacrylates and polymethacrylates in the literature.[36] It is noted that the presence of s-OCH_2 peaks is an evidence of gauche conformation of the EO side chains unlike oligo EO chains attached to a solid surface.[37] To confirm that dPS is not driving the segregation process—C−D bonds are less polarized and hence have a lower surface energy—the spectrum of an aromatic C−D stretching band of the 10% mixture of dPS−PME3MA in PS is plotted in Figure 7. No significant peaks are observed; the segregation process is not driven by the segregation of dPS but by the segregation of PME3MA blocks to the surface.

SFG spectra in a C−H stretching vibrations with SSP, PPP, and SPS polarization combinations are shown in Figure 8. Quantitative comparison of the peaks corresponding to s-OCH_3 at 2835 cm^{-1} in the spectra extracts the orientation of the methyl termini. The method of the quantitative analysis is described in the Appendix. Here we just show the result from the analysis. The polar tilt angle of $-CH_3$ is smaller than 30° when θ is assumed to have no angular distribution (δ-function approximation). For another extreme case in which θ = 0° on average is assumed, the standard deviation of

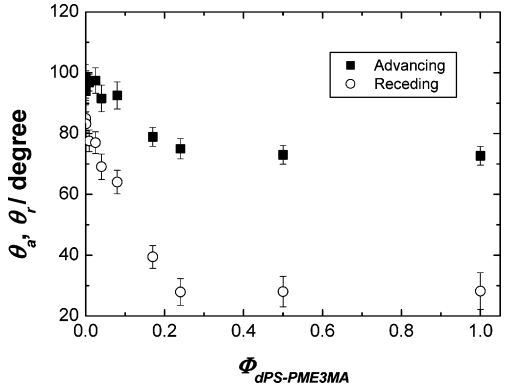

Figure 9. Advancing (■, θ_a) and receding (○, θ_r) contact angles of water on the surfaces of the mixtures of PS and dPS−PME3MA with volume fractions of $\Phi_{dPS-PME3MA}$. The error bars are standard deviations.

θ is found to be 26°. SFG unfortunately cannot distinguish those two cases, and thus the actual orientation should be somewhere between the two extreme cases. The side chains of PME3MA are, therefore, standing nearly normal to the surface and exposing the methyl termini to the surface. This conformation is compatible with the surface constraint which prefers exposing the lower surface energy fragments to the surface and hindering the hydrophilic high-energy part of the side chains from the surface.

Surface Reconstruction: Contact Angles. The mixtures of dPS−PME3MA and PS have extremely thin surface layers of hydrophobic methyl termini, barely covering the hydrophilic mobile EO side chains. Such hydrophobic surface may be unstable in a hydrophilic environment. Advancing and receding contact angles of water on the surface of the mixtures were measured and plotted in Figure 9. Both advancing and receding contact angles decrease with increasing amount of dPS−PME3MA; adding a small amount of dPS−PME3MA makes the surface hydrophilic. At the same time, the hysteresis between the advancing and receding contact angles becomes surprisingly large as the amount of dPS−PME3MA in the mixture increases. The advancing and receding contact angles as well as the hysteresis reach constant values at approximately 20%, which agrees very well with the concentration of dPS−PME3MA completely covering the surface as seen in Figure 4. The huge hysteresis is obviously related to the surface reconstruction of the PME3MA block. The side chains of PME3MA can reconstruct quickly since the methyl groups barely cover the hydrophilic EO side chains, which are mobile at room temperature. While the decreasing advancing angles may suggest the increasing surface enthalpy due to entropy driven surface segregation, even the advancing angles may be influenced by the quick surface reconstruction. In addition to the reconstruction of the side chains, the whole dPS−PME3MA block structure can be swollen by water so that the whole water-soluble PME3MA blocks are stretching out into water. Schematic pictures of possible conformations of dPS−PME3MA block copolymers at the surface (a vacuum/air) and water interface are shown in Figure 10. For this very unique property, the hierarchically nested amphiphilic structure, in which amphiphilic side chains are attached to an amphiphilic block copolymer, seems to be essential: the reconstruction of the side chains promotes the reconstruction of the entire block.

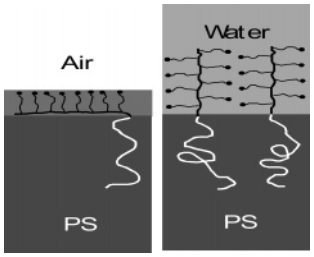

Figure 10. Schematic pictures of the conformations of dPS−PME3MA in a mixture with PS in air (or in a vacuum) and in water. At the surface in a vacuum or air, the terminal methyl groups of the side chains, ●, cover the surface. In water, the water-soluble PME3MA blocks are anchored onto the surface of polystyrene and stretching out into water. PME3MA blocks cover the surface in either hydrophobic or hydrophilic environment.

Summary

Segregation of dPS−PME3MA to the surface of PS provides the surface which is apparently hydrophobic but becomes hydrophilic upon contact with water. The segregation of dPS−PME3MA occurs even in hydrophobic environment and persist after prolonged annealing in a vacuum or air. The origin of such segregation is the presence of methyl termini of the side chains. Those methyl termini cover the surface, and the ethylene oxide part of the side chains are screened out from the surface. Once the surface is exposed to water, the surface reconstruction occurs quickly, and the wetting behavior of water changes drastically. Thanks to its block architecture with the hydrophobic block (PS in this study), the water-soluble PME3MA is expected to form a brush layer anchored to the surface of PS in water. Such a thermodynamically stable PME3MA surface layer in hydrophobic environment yet converting into a brush layer in water is an ideal candidate for biomedical applications. This unique character is due to the hierarchically nested amphiphilic architecture of the side chains and blocks.

Acknowledgment. We thank Daisuke Kawaguchi for his assistance for the neutron reflectivity measurement. This work was partially funded by the Project on Nanostructured Polymeric Materials of the New Energy and Industrial Technology Development Organization.

Appendix

In this appendix, we quantitatively analyze the SFG spectra with different polarization combinations. SFG spectra in the C−H stretching vibrations with SSP, PPP, and SPS polarization combinations shown in Figure 8 are quantitatively compared. The orientation of the methyl termini can be extracted from the peaks corresponding to s-OCH_3 at 2835 cm^{-1}. The intensity of sum frequency is proportional to the effective second-order nonlinear susceptibility, $\chi^{(2)}_{\text{eff}}$, as shown in eq A1. Note that the characters χ such as $\chi^{(2)}_{\text{eff}}$ and χ_{ijk} are exclusively used for susceptibility in this appendix to follow the conventional expression, while χ is used for the interaction parameters in main text.

$$I_{\text{SF}} \propto |\chi^{(2)}_{\text{eff}}|^2 I_{\text{vis}} I_{\text{IR}} \tag{A1}$$

$$\chi^{(2)}_{\text{eff}} = \chi^{(2)}_{\text{NR}} + \sum_q \frac{A_q}{\omega_{\text{IR}} - \omega_q + i\Gamma_q} \tag{A2}$$

I_{SF}, I_{vis}, and I_{IR} are the intensities of the sum-frequency, visible, and infrared light, respectively. $\chi^{(2)}_{\text{NR}}$ arises from the nonresonant background. The parameters ω_q, Γ_q, and A_q are the resonant frequency, homogeneous line width, and line strength of the vibrational mode q, respectively. Using eqs A1 and A2, the spectra are fit as shown as the solid lines in Figure 8 in order to obtain the sets of parameters listed in Table 1. The effective second-order nonlinear susceptibility of the surface $\chi^{(2)}_{\text{eff}}$ measured with a polarization combination is a function of the Fresnel coefficients, L_{ii} ($i = x$, y, or z), incident and takeoff angles of light, and the second nonlinear susceptibilities, χ_{ijk} ($i, j, k = x, y,$ or z) in a lab coordinate. In particular, for SSP and PPP polarizations, the effective susceptibilities are

$$\chi^{(2)}_{\text{eff·SSP}} = L_{yy}(\omega_{\text{SF}})\, L_{yy}(\omega_{\text{vis}})\, L_{zz}(\omega_{\text{IR}}) \sin\beta_{\text{IR}} \chi_{yyz} \tag{A3}$$

$$\begin{aligned}\chi^{(2)}_{\text{eff·PPP}} = {} & -L_{xx}(\omega_{\text{SF}})\, L_{xx}(\omega_{\text{vis}})\, L_{zz}(\omega_{\text{IR}}) \cos\beta_{\text{SF}} \cos\beta_{\text{vis}} \sin\beta_{\text{IR}} \chi_{xxz} - L_{xx}(\omega_{\text{SF}})\, L_{zz}(\omega_{\text{vis}})\, L_{xx}(\omega_{\text{IR}}) \cos\beta_{\text{SF}} \sin\beta_{\text{vis}} \cos\beta_{\text{IR}} \chi_{xzx} + \\ & L_{zz}(\omega_{\text{SF}})\, L_{xx}(\omega_{\text{vis}})\, L_{xx}(\omega_{\text{IR}}) \sin\beta_{\text{SF}} \sin\beta_{\text{vis}} \sin\beta_{\text{IR}} \chi_{zxx} + L_{zz}(\omega_{\text{SF}})\, L_{zz}(\omega_{\text{vis}})\, L_{zz}(\omega_{\text{IR}}) \sin\beta_{\text{SF}} \sin\beta_{\text{vis}} \sin\beta_{\text{IR}} \chi_{zzz}\end{aligned} \tag{A4}$$

The lab coordinates x, y, and z are chosen such that z is the surface normal and x is in the incident plane. The Fresnel coefficients are given by the following equations:

$$L_{xx}(\omega_{\text{p}}) = \frac{2n_{\text{air}}(\omega_{\text{p}}) \cos\beta_{\text{p,polym}}}{n_{\text{air}}(\omega_{\text{p}}) \cos\beta_{\text{p,polym}} + n_{\text{polym}}(\omega_{\text{p}}) \cos\beta_{\text{p,air}}}$$

$$L_{yy}(\omega_{\text{p}}) = \frac{2n_{\text{air}}(\omega_{\text{p}}) \cos\beta_{\text{p,air}}}{n_{\text{air}}(\omega_{\text{p}}) \cos\beta_{\text{p,air}} + n_{\text{polym}}(\omega_{\text{p}}) \cos\beta_{\text{p,polym}}}$$

$$L_{zz}(\omega_{\text{p}}) = \frac{2n_{\text{polym}}(\omega_{\text{p}}) \cos\beta_{\text{p,air}}}{n_{\text{air}}(\omega_{\text{p}}) \cos\beta_{\text{p,polym}} + n_{\text{polym}}(\omega_{\text{p}}) \cos\beta_{i,\text{air}}} \left(\frac{n_{\text{air}}(\omega_{\text{p}})}{n'(\omega_{\text{p}})}\right)^2 \tag{A5}$$

where β_{p} and ω_{p} are the incident angle and frequency of p-light, respectively (p is either a sum-frequency (SF), visible (vis), or infrared (IR) light). A hypothetical refractive index of the interface is denoted as n', which

Table 1. Peak Assignments and the Parameters Computed from the Data Fitting of Figure 8

ω_q (cm^{-1})	Γ_q (cm^{-1})	A_{ssp}	A_{ppp}	A_{sps}	assignment
2835	12	1.76 ± 0.05	1.72 ± 0.05	0.04 ± 0.01	s-OCH_3(r^+)
2873	10	3.30 ± 0.05	2.08 ± 0.05	0.03 ± 0.01	s-OCH_2(d^+)
2910	15	1.65 ± 0.10	2.17 ± 0.05	0.44 ± 0.02	CH_2
2940	10	1.66 ± 0.05	0.47 ± 0.02	0.02 ± 0.01	as-OCH_2(d^-)
2965	10	1.10 ± 0.05	1.88 ± 0.05	1.66 ± 0.05	as-OCH_3(r^-)

is an unknown parameter. For CH_3 having C_{3v} symmetry, one obtains the susceptibilities as follows:[38]

$$\chi_{xxz} = \chi_{yyz} = \frac{1}{2}N\alpha_{ccc}(\langle\cos\theta\rangle(1+r) - \langle\cos^3\theta\rangle(1-r)) \quad \text{(A6)}$$

$$\chi_{xzx} = \chi_{yzy} = \chi_{zxx} = \chi_{zyy} = \frac{1}{2}N\alpha_{ccc}(\langle\cos\theta\rangle - \langle\cos^3\theta\rangle)(1-r) \quad \text{(A7)}$$

$$\chi_{zzz} = N\alpha_{ccc}(\langle\cos\theta\rangle + \langle\cos^3\theta\rangle)(1-r) \quad \text{(A8)}$$

where N, θ, α_{ccc}, and r are the surface density of methyl group, angle between the c axis of CH_3 and the surface normal, methyl symmetric stretch hyperpolarization tensor component in Euler angle, and ratio of hyperpolarizability, $\alpha_{aac}/\alpha_{ccc}$, respectively. The c axis is chosen to be parallel to the O−C bond of the methoxy group while the choice of a and b is arbitrary due to the symmetry of CH_3. In consequence, A_q(PPP)/A_q(SSP) is a function of θ, r, and n'. Using an apparent refractive index of the surface layer, $n' = 1.05$, and the ratio of hyperpolarizability of s-OCH_3, $r = 1.66$,[39,40] we are able to compute A_q(PPP)/A_q(SSP) as a function of θ. The details of the method of estimating n' and r are found in the Supporting Information. s-CH_3 is assumed to orient an average polar tilt angle θ_0 respective to the surface normal with standard deviation σ. A_q(PPP)/A_q(SSP) is computed by assuming a Gaussian distribution of polar tilt angles as shown in eq A9:

$$f(\theta) = C\exp[-(\theta-\theta_0)^2/2\sigma^2] \quad \text{(A9)}$$

where C is a constant. $\sigma = 0$ corresponds to the δ-function distribution of polar tilt angle. The result of the computation is shown in Figure 11. The horizontal

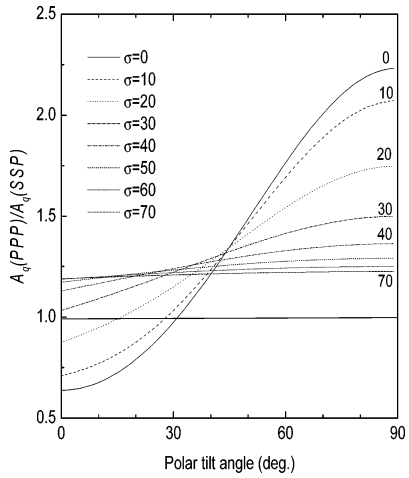

Figure 11. Ratio of line strengths of A_q(PPP) and A_q(SSP) of the mixture of PS and dPS−PME3MA (10%). The solid linear line indicates the value experimentally observed. The possible combinations of θ_0 and σ are found from the cross section of the solid line and the curves with various σ.

solid straight line indicates the experimentally obtained value and the curve assuming δ-function distribution cross the solid line at θ of 30°. The polar tilt angle cannot be larger than 30° but smaller when the δ-function approximation is not valid. For an extreme case of $\theta = 0$, σ is about 26°, which is another extreme case of the possible scenarios.

Supporting Information Available: Details of the method of estimating n' and r. This material is available free of charge via the Internet at http://pubs.acs.org.

References and Notes

(1) Tirrell, M.; Kokkoli, E.; Biesalski, M. *Surf. Sci.* **2002**, *500*, 61. Elbert, D. L.; Hubbell, J. A. *Annu. Rev. Mater. Sci.* **1996**, *26*, 365. Klee, D.; Hoecker, H. *Adv. Polym. Sci.* **1999**, *149*, 1. Griffith, L. G. *Acta Mater.* **2000**, *48*, 263. Langer, R.; Vacanti, J. P. *Science* **1993**, *260*, 920. Hubbell, J. A. *Curr. Opin. Biotechnol.* **1999**, *10*, 123. Hubbell, J. A. *BioTechnology* **1995**, *13*, 565. Peppas, N. A.; Langer, R. *Science* **1994**, *263*, 1715. Williams, D. F., Ed.; *Definitions in Biomaterials*, *Progress in Biomedical Engineering*; Elsevier: Amsterdam, 1987; Vol. 4.

(2) Andrade, J. D.; Hlady, V. *Adv. Polym. Sci.* **1986**, *79*, 1. Horbett, T. A. *Cardiovasc. Pathol.* **1993**, *2*, 137. Luscher, E. F.; Weber, S. *Thromb. Haemostasis* **1993**, *70*, 234. Brash, J. L. *J. Biomater. Sci., Polym. Ed.* **2000**, *11*, 1135.

(3) Topoglidis, E.; Cass, A. E. G.; Gilardi, G.; Sadeghi, S.; Beaumont, N.; Durrant, J. R. *Anal. Chem.* **1998**, *70*, 5111. Ghose, S.; Chase, H. *Bioseparation* **2000**, *9*, 21. Shi, H. Q.; Ratner, B. D. *J. Biomed. Mater. Res.* **2000**, *49*, 1. Wang, N. H. L. *J. Cell. Biochem.* **1993**, *Suppl. 17A*, 43. Nyquist, R. M.; Eberhardt, A. S.; Silks, L. A.; Li, Z.; Yang, X.; Swanson, B. I. *Langmuir* **2000**, *16*, 1793. Sukhishvili, S. A.; Granick, S. *J. Chem. Phys.* **1999**, *110*, 10153.

(4) Ratner, B. D. *J. Biomater. Sci. Polym. Ed.* **2000**, *11*, 110719. Mori, Y.; Nagaoka, S.; Takiuchi, H.; Kikuchi, T.; Noguchi, N.; Tanzawa, H.; Noishiki, Y. *Trans. ASAIO* **1982**, *28*, 459.

(5) Shen, M.; Martinson, L.; Wagner, M. S.; Castner, D. G.; Ratner, B. D.; Horbett, T. A. *J. Biomater. Sci., Polym. Ed.* **2002**, *13*, 367.

(6) Harder, P.; Grunze, M.; Dahint, R.; Whitesides, G. M.; Laibinis, P. E. *J. Phys. Chem. B* **1998**, *102*, 426. Tokumitsu, S.; Liebich, A.; Herrwerth, S.; Eck, W.; Himmelhaus, M.; Grunze, M. *Langmuir* **2002**, *18*, 8862.

(7) Feldman, K.; Hahner, G.; Spencer, N. D.; Harder, P.; Grunze, M. *J. Am. Chem. Soc.* **1999**, *121*, 10134. Jeon, S. I.; Lee, J. H.; Andrade, J. D.; deGennes, P. G. *J. Colloid Interface Sci.* **1991**, *142*, 149.

(8) Zhao, B.; Brittain, W. J. *Prog. Polym. Sci.* **2000**, *25*, 677.

(9) Chen, W.-L.; Shull, K. R. *Macromolecules* **1999**, *32*, 6298.

(10) Peppas, N. A.; Huang, Y.; Torres-Lugo, M.; Ward, J. H.; Zhang, J. *Annu. Rev. Biomed. Eng.* **2000**, *2*, 9.

(11) Iyengar, D. R.; Perutz, S. M.; Dai, C.-A.; Ober, C. K.; Kramer, E. J. *Macromolecules* **1996**, *29*, 1229.

(12) Lewis, K. B.; Ratner, B. D. *J. Colloid Interface Sci.* **1993**, *159*, 77. Shard, A. G.; Davies, M. C.; Li, Y. X.; Volland, C.; Kissel, T. *Macromolecules* **1997**, *30*, 3051.

(13) Kajiyama, T.; Teraya, T.; Takahara, A. *Polym. Bull. (Berlin)* **1990**, *24*, 333. Yuan, Y.; Shoichet, M. S. *Macromolecules* **2000**, *33*, 4926.

(14) Walton, D. G.; Soo, P. P.; Mayes, A. M.; Sofia Allgor, S. J.; Fujii, J. T.; Griffith, L. G.; Ankner, J. F.; Kaiser, H.; Johansson, J.; Smith, G. D.; Barker, J. G.; Satija, S. K. *Macromolecules* **1997**, *30*, 6947.

(15) Han, S.; et al. Manuscript in preparation.

(16) Han, S.; Hagiwara, M.; Ishizone, T. *Macromolecules* **2003**, *36*, 8312.

(17) Ashley, J. C. *J. Electron Spectrosc. Relat. Phenom.* **1982**, *28*, 177.

(18) Yokoyama, H.; Tanaka, K.; Takahara, A.; Kajiyama, T.; Sugiyama, K.; Hirao, A. *Macromolecules* **2004**, *37*, 939.

(19) Torikai, N.; Furusaka, M.; Matsuoka, H.; Matsushita, Y.; Shibayama, M.; Takahara, A.; Takeda, M.; Tasaki, S. Yamaoka, H. *Appl. Phys. A* **2002**, *74*, S264.

(20) Welp, K. A.; Co, C. C.; Wool, R. P. *J. Neutron Res.* **1999**, *8*, 37.

(21) Miyamae, T.; Tsukagoshi, K.; Matsuoka, O.; Yamamoto, S.; Nozoye, H. *Langmuir* **2001**, *17*, 8125.

(22) Leibler, L. *Macromolecules* **1980**, *13*, 1602.

(23) χ, R_g, and C are randomly chosen from possible ranges of values to find the set of parameters with minimum deviations from the data.

(24) The long side chain of PME3MA reduces the number of segments per molecular weight but increases chain stiffness. R_g/(molecular weight)$^{1/2}$ is therefore a weak decreasing function of the degree of branching, and the assumption slightly overestimates R_g.

(25) Fredrickson, G. H. *Macromolecules* **1987**, *20*, 2535. Anastasiadis, S. H.; Russell, T. P.; Satija, S. K.; Majkrzak, C. F. *Phys. Rev. Lett.* **1989**, *62*, 1852. Menelle, A.; Russell, T. P.; Anas-

tasiadis, S. H.; Satija, S. K.; Majkrzak, C. F. *Phys. Rev. Lett.* **1992**, *68*, 67.
(26) Semenov, A. N. *Macromolecules* **1992**, *25*, 4967.
(27) Leibler, L. *Makromol. Chem., Macromol. Symp.* **1988**, *16*, 1.
(28) Shull, K. R.; Winey, K. I.; Thomas, E. L.; Kramer, E. J. *Macromolecules* **1991**, *24*, 2748.
(29) Briggman, K. A.; Stephenson, J. C.; Wallace, W. E.; Richter, L. J. *J. Phys. Chem. B* **2001**, *105*, 2785. Gautam, K. S.; Schwab, A. D.; Dhinojwala, A.; Zhang, D.; Dougal, S. M.; Yeganeh, M. S. *Phys. Rev. Lett.* **2000**, *85*, 3854.
(30) Brandrup, J., Immergut, E. H., Grulke, E. A., Abe, A., Bloch, D. R., Eds. *Polymer Handbook*, 4th ed.; John Wiley & Sons: New York, 1999.
(31) Miranda, P. B.; Shen, Y. R. *J. Phys. Chem. B* **1999**, *103*, 3292. Richmond, G. L. *Anal. Chem.* **1997**, *69*, 9, A536. Bain, C. D. *J. Chem. Soc., Faraday Trans.* **1995**, *91*, 1281. Himmelhaus, M.; Eisert, F.; Buck, M.; Grunze, M.; *J. Phys. Chem. B* **2000**, *104*, 576.
(32) Wei, X.; Zhuang, X.; Hong, S.-C.; Goto, T.; Shen, Y. R. *Phys. Rev. Lett.* **1999**, *82*, 4256. Zhang, D.; Shen, Y. R.; Somorjai, G. *Chem. Phys. Lett.* **1997**, *281*, 394. Gracias, D. H.; Zhang, D.; Lianos, L.; Ibach, W.; Shen, Y. R.; Somorjai, G. A. *Chem. Phys.* **1999**, *245*, 277.
(33) Chen, Z.; Ward, R.; Tian, Y.; Eppler, A. S.; Shen, Y. R.; Somorjai, G. A. *J. Phys. Chem. B* **1999**, *103*, 2935.
(34) Kim, D.; Shen, Y. R. *Appl. Phys. Lett.* **1999**, *74*, 3314.
(35) Dreesen, L.; Humbert, C.; Hollander, P.; Mani, A. A.; Ataka, K.; Thiry, P. A.; Peremans, A. *Chem. Phys. Lett.* **2001**, *333*, 327. Chen, Z.; Ward, R.; Tian, Y.; Baldelli, S.; Opdahl, A.; Shen, Y.-R.; Somorjai, G. A. *J. Am. Chem. Soc.* **2000**, *122*, 10615. Ye, S.; Morita, S.; Li, G.; Noda, H.; Tanaka, M.; Uosaki, K.; Osawa, M. *Macromolecules* **2003**, *36*, 5694. Chen, C.; Loch, C. L.; Wang, J.; Chen, Z. *J. Phys. Chem. B* **2003**, *107*, 10440.
(36) Wang, J.; Chen, C.; Buck, S. M.; Chen, Z. *J. Phys. Chem. B* **2001**, *105*, 12118. Chen, C.; Wang, J.; Woodcock, S. E.; Chen, Z. *Langmuir* **2002**, *18*, 1302.
(37) Zolk, M.; Eisert, F.; Pipper, J.; Herrwerth, S.; Eck, W.; Buck, M.; Grunze, M. *Langmuir* **2000**, *16*, 5849.
(38) Hirose, C.; Akamatsu, N.; Domen, K. *Appl. Spectrosc.* **1992**, *46*, 1051.
(39) n' and r are typically chosen in the range of 1.0 to n (the refractive index of bulk material) and 1.6 to 4.2, respectively. We selected n' and r from the range so that the simulation is consistent with the experimental results.
(40) Iimori, T.; Iwahashi, T.; Ishii, H.; Seki, K.; Ouchi, Y.; Ozawa, R.; Hamaguchi, H.; Kim, D. *Chem. Phys. Lett.* **2004**, *389*, 321326. Oh-e, M.; Yokoyama, H.; Baldelli, S. *Appl. Phys. Lett.* **2004**, *84*, 4965. Ye, S.; Morita, S.; Li, G.; Noda, H.; Tanaka, M.; Uosaki, K.; Osawa, M. *Macromolecules* **2003**, *36*, 5694.

MA050473W